JACS
JOURNAL OF THE AMERICAN CHEMICAL SOCIETY
Communication
pubs.acs.org/JACS

# Pressure-Induced Metallization of the Halide Perovskite $(CH_3NH_3)PbI_3$

Adam Jaffe,[†] Yu Lin,[†,§] Wendy L. Mao,[*,‡,§] and Hemamala I. Karunadasa[*,†]

Departments of [†]Chemistry and [‡]Geological Sciences, Stanford University, Stanford, California 94305, United States
[§]Photon Science and Stanford Institute for Materials and Energy Sciences, SLAC National Accelerator Laboratory, Menlo Park, California 94025, United States

Supporting Information

**ABSTRACT:** We report the metallization of the hybrid perovskite semiconductor (MA)$PbI_3$ (MA = $CH_3NH_3^+$) with no apparent structural transition. We tracked its bandgap evolution during compression in diamond-anvil cells using absorption spectroscopy and observed strong absorption over both visible and IR wavelengths at pressures above ca. 56 GPa, suggesting the imminent closure of its optical bandgap. The metallic character of (MA)$PbI_3$ above 60 GPa was confirmed using both IR reflectivity and variable-temperature dc conductivity measurements. The impressive semiconductor properties of halide perovskites have recently been exploited in a multitude of optoelectronic applications. Meanwhile, the study of metallic properties in oxide perovskites has revealed diverse electronic phenomena. Importantly, the mild synthetic routes to halide perovskites and the templating effects of the organic cations allow for fine structural control of the inorganic lattice. Pressure-induced closure of the 1.6 eV bandgap in (MA)$PbI_3$ demonstrates the promise of the continued study of halide perovskites under a range of thermodynamic conditions, toward realizing wholly new electronic properties.

Halide perovskites are a family of crystalline solids that exhibit exceptional semiconductor properties. These properties have been leveraged in various optoelectronic applications such as photovoltaics,[1] light-emitting diodes,[2] and white-light phosphors.[3] The three-dimensional hybrid perovskite (MA)$PbI_3$ (MA = $CH_3NH_3^+$) has recently been used as a light absorber in low-cost and high-efficiency solar cells owing to its solution-state synthesis, direct bandgap ($E_g$) of ca. 1.6 eV, and long carrier lifetime and diffusion length.[1] Notably, halide perovskites have compressible lattices and their electronic properties display a large pressure response.[4] Lattice compression can promote exotic behavior in solids, including induced[5] or enhanced[6] superconductivity, magnetic ordering,[7] and metallization.[8] Indeed decades of high-pressure investigations of semiconductors have afforded valuable insight into their electronic properties. High-pressure studies also provide important experimental calibration for theoretical models of solid-state properties that rely on interatomic distances—a parameter that can be systematically varied with lattice compression.[9] While oxide perovskites exhibit diverse electronic structures ranging from insulators to superconductors, all two- and three-dimensional halide perovskites reported to date have bandgaps of ca. 1−3 eV. Therefore, pressure is an important dial for accessing still greater electronic diversity from this large and tunable family of materials.

We recently tracked how the pressure-induced structural evolution of (MA)$PbI_3$ corresponded to changes in its photophysical and transport properties using high-pressure single-crystal and powder X-ray diffraction (PXRD), photoluminescence, and conductivity measurements obtained during compression of the perovskite in diamond-anvil cells (DACs).[10] Several other studies have also investigated the behavior of this perovskite upon compression, albeit in relatively low-pressure regimes (below 10 GPa).[4a,b,11] To our knowledge, the optical absorption of (MA)$PbI_3$ has only been measured up to 4.4 GPa[11d] and compression below this pressure has only tuned its bandgap by ca. 0.3 eV.[10,11] Notably, our room-temperature resistivity measurements up to ca. 50 GPa showed a rapid increase in conductivity above 30 GPa, yielding a maximum of 1.5 $S \cdot cm^{-1}$ at 51 GPa.[10] This conductivity increase was accompanied by a decrease in the activation energy ($E_a$) of conduction (from 19.0(8) meV at 47 GPa down to 13.2(3) meV at 51 GPa). The trends of increasing conductivity and decreasing $E_a$ suggested an eventual metallic transition at higher pressures. However, the material's properties above 51 GPa have not been reported. Herein, we report the metallization of (MA)$PbI_3$ through apparent bandgap closure at pressures above 60 GPa. We track this metallic transition using high-pressure absorption spectroscopy, IR reflectivity, and temperature-dependent four-point dc conductivity measurements. This semiconductor-to-metal transition indicates the realization of a new electronic structure and transport properties in this technologically important hybrid material.

We tracked the bandgap evolution of (MA)$PbI_3$ during compression in DACs by measuring absorption spectra across visible and IR wavelengths (Figures 1, S1, and S2). Pressure values were measured using ruby fluorescence and their errors (of ca. 5%) are discussed in the Supporting Information. Our lower-pressure measurements are consistent with prior reports of the material's optical behavior under pressure.[10,11] Previous work showed an initial bandgap redshift during compression within the low-pressure $\alpha$ phase, followed by blueshifting during and after transitioning to the cubic $\beta$ phase above 0.3 GPa.[10,11] Subsequent compression within the $\beta$ phase was then shown to yield a slight bandgap redshift, followed by further blueshifting upon the onset of the high-pressure, partially amorphous $\gamma$ phase at ca. 3 GPa.[10,11b−d] These changes were

**Received:** February 2, 2017
**Published:** March 14, 2017





DOI: 10.1021/jacs.7b01162
J. Am. Chem. Soc. XXXX, XXX, XXX−XXX

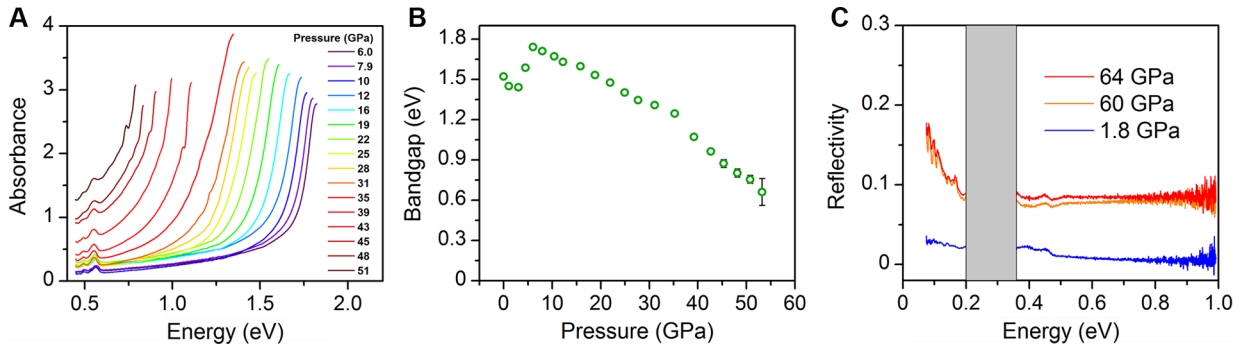


**Figure 1.** (A) Variable-pressure optical absorption spectra for $(MA)PbI_3$ at visible and IR wavelengths, showing the redshift of the direct bandgap ($E_g$) with increasing pressure above 6.0 GPa. (B) $E_g$ as a function of pressure calculated from direct-bandgap Tauc plots. (C) Reflectivity of $(MA)PbI_3$–diamond above the metallization pressure (orange and red lines), showing Drude-like modes at low frequency, diagnostic of metallic behavior. The reflectivity spectrum at low pressure is shown for comparison (blue line). Strong diamond absorption occurs in the gray region.

reported for the relatively low-pressure regime from ambient pressure up to 4.4 GPa. Here, we show that with further compression within the partially amorphous $\gamma$ phase, the bandgap continues to blueshift until 6.0 GPa (Figures 1B and S1). Above 6.0 GPa, the $E_g$ continually decreases with increasing pressure (Figure 1A,B). At ca. 35 GPa, a slight discontinuity in the evolution of $E_g$ during compression occurs (Figure 1B), after which $E_g$ decreases more rapidly with increasing pressure. Interestingly, we previously found that the electronic conductivity of $(MA)PbI_3$ sharply increases upon compression above ca. 35 GPa,[10] corroborating altered electronic behavior at this pressure. Bandgap determination becomes difficult above 51 GPa because of strong absorption (Figure S2).

Considering the strong absorption above ca. 56 GPa, even at low energies, we measured IR reflectivity to determine if the material had undergone a transition from semiconducting to metallic behavior. Indeed, at 60 GPa we observe a Drude-like mode[9] below ca. 0.2 eV, showing sharply increasing reflectivity with decreasing frequency, in contrast to a spectrum recorded at lower pressure (Figure 1C). This indicates the transition of $(MA)PbI_3$ to a metallic state. We observe a slight increase in overall reflectivity with further compression to 64 GPa, the highest pressure for which we measured spectra.

To independently confirm the transition of $(MA)PbI_3$ from a semiconductor to a metal, we measured its temperature-dependent dc conductivity under pressure. The measurement was performed using a four-point electrode configuration to eliminate contact resistance. In a semiconductor, electronic conductivity ($\sigma$) increases with increasing temperature ($T$). In this case, electronic conductivity follows Arrhenius behavior, yielding a linear relationship between $\ln(\sigma)$ and $T^{-1}$. The slope of this line gives $-E_a/R$, where $R$ is the gas constant and $E_a$ is the activation energy of conduction. In contrast, metallic systems show decreases in $\sigma$ with increasing temperature due to increased carrier scattering induced by lattice vibrations.

The temperature-dependent conductivity of $(MA)PbI_3$ at 50 GPa is consistent with our prior results obtained at similar pressures.[10] At this pressure, we obtain a room-temperature conductivity value of 0.57 $S{\cdot}cm^{-1}$. A linear fit of the Arrhenius relation (Figure 2) gives an $E_a$ of conduction of 19.2(3) meV, indicating that the material is still semiconducting. We then compressed the material above pressures for which optical reflectivity measurements indicated the transition to metallic behavior. At 62 GPa, we measure room-temperature conductivity of 6.6 $S{\cdot}cm^{-1}$. Furthermore, the conductivity now

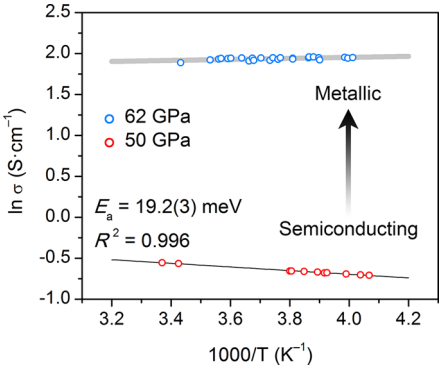


**Figure 2.** Arrhenius plot of the temperature dependence of conductivity in $(MA)PbI_3$ at 50 (red) and 62 GPa (blue). At 50 GPa, the conductivity shows the expected behavior for a semiconductor, with higher conductivity at higher temperature. A linear fit yields an activation energy ($E_a$) of conduction of 19.2(3) meV. At 62 GPa, $(MA)PbI_3$ shows decreasing conductivity with increasing temperatures (a gray bar is drawn to guide the eye), indicative of metallic behavior, where conduction is not thermally activated.

decreases with increasing temperature (Figure 2), confirming the absence of thermally activated conduction. This behavior is a hallmark of metallic character.

Based on a simple linear extrapolation of $E_g$ as a function of pressure (Figure S3), $(MA)PbI_3$ should not metallize through bandgap closure until ca. 75 GPa. To determine if a structural phase transition was responsible for the earlier onset of metallic behavior at 60 GPa, we obtained PXRD data on $(MA)PbI_3$ up to 66 GPa (Figure S4). Previous work has shown that $(MA)PbI_3$ undergoes a phase transition at ca. 0.3 GPa ($\alpha$ to $\beta$ phase), followed by the onset of partial amorphization between 2.5 and 2.9 GPa ($\beta$ to $\gamma$ phase).[10,11b–d] With continued compression, we previously reported that this partially amorphous $\gamma$ phase, where some crystalline reflections are maintained, is retained up to ca. 50 GPa.[10] In our current PXRD measurements up to 66 GPa, we continue to see no evidence of a first-order structural phase transition, as reflected by the monotonic evolution of the diffraction peak positions and amorphous signature with compression. However, decreases in octahedral tilting and increases in Pb–I bond compression could yield nonlinear decreases in $E_g$ without causing changes to overall lattice symmetry (similar to the discontinuity observed at ca. 35 GPa). Since the material is partially amorphous, structural changes on a more local scale


DOI: 10.1021/jacs.7b01162
J. Am. Chem. Soc. XXXX, XXX, XXX–XXX

may also play a role in the metallization onset. Additionally, non-hydrostatic pressure conditions may cause portions of the sample to experience higher stress than the bulk, leading to early metallization. Similar to our previous report that the pressure-induced structural and optical changes in $(MA)PbI_3$ are reversible,[10] we find that the original $\alpha$ phase is recovered upon decompression from 66 GPa back to ambient pressure (Figure S5). This reversibility indicates that the metallization is likely not a result of irreversible material decomposition.

All materials are expected to eventually become metallic, given sufficient compression.[12] Compression can increase orbital overlap, leading to increased band dispersion. However, the pressure responses of electronic bands and their positions relative to each other are also dictated by the structure and bulk symmetry of a particular material. Therefore, the pressures at which metallization occurs through bandgap closure can vary enormously depending on material structure and composition. We previously reported the electronic structure for the crystalline $\beta$ phase of $(MA)PbI_3$.[10] Similar to its $\alpha$-phase band structure, here too the valence-band maximum is predominantly derived from I 5p states (mixed with Pb 6s states) while the conduction-band minimum is primarily Pb 6p in character. Bandgap closure above ca. 60 GPa in the $\gamma$ phase thus likely involves overlap of these band edges, although the precise physical and electronic structure of the partially amorphous $\gamma$ phase remains to be elucidated.

Bandgap closure allows for electronic itinerancy, which, when combined with electron−electron correlations and electron−phonon coupling (observed in these soft metal halide lattices)[13] has been implicated in transport phenomena such as superconductivity. Indeed, the coupling of charge carriers to the lattice (or polaron formation) has been invoked to explain unusual characteristics in halide perovskites, such as long carrier lifetimes in 3D perovskites[14] and white-light emission from 2D perovskites.[3] Furthermore, the perovskites $CsPbI_3$ and $CsSnI_3$ have been predicted to become topological insulators (bulk insulators with metallic surface states) under high pressure,[15] which requires gapless surface states.

Material compression has led to large increases in conductivity in 2D Cu−Cl perovskites[16] and decreased the bandgaps of 2D Pb−I[17] and Pb−I−SCN[18] perovskites down to ca. 2 eV. Similarly, the bandgaps of the 3D perovskites $(MA)PbI_3$,[10,11] $(MA)PbBr_3$,[17b] $(FA)PbBr_3$[19] ($FA = H_2NCH{=}NH_2^+$), and $(FA)PbI_3$[20] have been tuned by ca. 0.3 eV in relatively low pressure regimes. Importantly, in many of these cases the $E_g$ increases with mild compression and in all cases these materials remain as semiconductors at the pressures studied. Metallic conductivity has been reported in the tin perovskites $ASnI_3$ (A = MA, FA, Cs) at ambient pressure.[21] However, these materials have bandgaps of ca. 1.3 eV and the source of the high conductivity has not been linked to bandgap closure. Instead, conductivity arises from spontaneous hole doping through the facile oxidation of the Sn 5s-based valence band, affording empty states at the top of this highly dispersed band.[21d,22] To our knowledge, the only halide perovskites previously reported to show bandgap closure at high pressures are the mixed-valence double perovskites: $Cs_2Au^{I}Au^{III}X_6$ (X = $Cl^-$, $Br^-$, or $I^-$).[23] Here, electronic delocalization between the gold centers at high pressures is thought to contribute to the conductivity.[23]

In contrast to halide perovskites, the transport properties of oxide perovskites have been studied for decades to yield extremely diverse electronic platforms: insulators, semiconductors, conductors, and even high-temperature superconductors.[24] Although high-temperature routes (often well above 500 °C) are commonly required to synthesize oxide perovskites,[25] judicious choice of inorganic ions can exert substantial structural control over the lattice.[26] The solution-state syntheses of halide perovskites under ambient conditions allow for additional control of the inorganic lattice through templating interactions with organic cations that can be systematically varied. Herein, we have shown that the hybrid perovskite $(MA)PbI_3$, which has come under intense recent scrutiny for its exceptional photovoltaic and other optoelectronic properties, exhibits wholly new transport properties at pressures of ca. 60 GPa. At this pressure and above, $(MA)PbI_3$ exhibited a Drude-like mode at low frequency in IR reflectivity measurements, which is diagnostic of a metallic state. As independent confirmation of metallic character, metallic conduction behavior was observed in variable-temperature dc conductivity measurements. Our work demonstrates that the bandgap of $(MA)PbI_3$ can be continuously decreased from 1.6 to ca. 0 eV through compression and motivates further exploration of the high-pressure behavior of the large and diverse family of halide perovskites.

## ■ ASSOCIATED CONTENT

### Supporting Information

The Supporting Information is available free of charge on the ACS Publications website at DOI: 10.1021/jacs.7b01162.

Experimental details, diffraction patterns, and spectra, including Figures S1−S5 (PDF)

## ■ AUTHOR INFORMATION


### Corresponding Authors

*wmao@stanford.edu

*hemamala@stanford.edu

### ORCID

Adam Jaffe: 0000-0002-9886-0249

Hemamala I. Karunadasa: 0000-0003-4949-8068


### Notes

The authors declare no competing financial interest.

## ■ ACKNOWLEDGMENTS

Work by A.J. and H.K. was funded by the National Science Foundation (NSF) CAREER award DMR-1351538. Work by Y.L. and W.M. was supported through the U.S. Department of Energy (DOE) through the Stanford Institute for Materials & Energy Sciences DE-AC02-76SF00515. A.J. is supported by the Stanford Chemistry William S. Johnson Fellowship. High-pressure absorption and reflectivity spectra were collected at the Infrared Laboratory of the National Synchrotron Light Source II, a DOE Office of Science User Facility operated by Brookhaven National Laboratory under Contract No. DE-SC0012704. The Infrared Laboratory is supported by the Consortium for Materials Properties Research (COMPRES) in Earth Sciences under NSF Cooperative Agreement EAR 1606856 and the DOE/National Nuclear Security Administration under Grant DE-NA-0002006, Carnegie DOE Alliance Center. High-pressure PXRD was performed at beamline 12.2.2 at the Advanced Light Source (ALS). The ALS is supported by the Director, Office of Science, Office of Basic Energy Sciences, of the DOE under Contract No. DE-AC02-05CH11231. The high-pressure facilities at the ALS are supported by COMPRES



DOI: 10.1021/jacs.7b01162
J. Am. Chem. Soc. XXXX, XXX, XXX−XXX

under NSF Cooperative Agreement EAR 11-57758. We thank Drs. Zhenxian Liu, Martin Kunz, and Christine Beavers for experimental assistance.

## REFERENCES

(1) (a) Kojima, A.; Teshima, K.; Shirai, Y.; Miyasaka, T. *J. Am. Chem. Soc.* **2009**, *131*, 6050. (b) Green, M. A.; Ho-Baillie, A.; Snaith, H. J. *Nat. Photonics* **2014**, *8*, 506. (c) Kazim, S.; Nazeeruddin, M. K.; Grätzel, M.; Ahmad, S. *Angew. Chem., Int. Ed.* **2014**, *53*, 2812.
(2) Tan, Z.-K.; Moghaddam, R. S.; Lai, M. L.; Docampo, P.; Higler, R.; Deschler, F.; Price, M.; Sadhanala, A.; Pazos, L. M.; Credgington, D.; Hanusch, F.; Bein, T.; Snaith, H. J.; Friend, R. H. *Nat. Nanotechnol.* **2014**, *9*, 687.
(3) Dohner, E. R.; Jaffe, A.; Bradshaw, L. R.; Karunadasa, H. I. *J. Am. Chem. Soc.* **2014**, *136*, 13154.
(4) (a) Onoda-Yamamuro, N.; Yamamuro, O.; Matsuo, T.; Suga, H. *J. Phys. Chem. Solids* **1992**, *53*, 277. (b) Gesi, K. *Ferroelectrics* **1997**, *203*, 249. (c) Smith, I. C.; Smith, M. D.; Jaffe, A.; Lin, Y.; Karunadasa, H. I. *Chem. Mater.* **2017**, *29*, 1868.
(5) (a) Drozdov, A. P.; Eremets, M. I.; Troyan, I. A.; Ksenofontov, V.; Shylin, S. I. *Nature* **2015**, *525*, 73. (b) Torikachvili, M. S.; Bud'ko, S. L.; Ni, N.; Canfield, P. C. *Phys. Rev. Lett.* **2008**, *101*, 057006.
(6) Gao, L.; Xue, Y. Y.; Chen, F.; Xiong, Q.; Meng, R. L.; Ramirez, D.; Chu, C. W.; Eggert, J. H.; Mao, H. K. *Phys. Rev. B: Condens. Matter Mater. Phys.* **1994**, *50*, 4260.
(7) Egan, L.; Kamenev, K.; Papanikolaou, D.; Takabayashi, Y.; Margadonna, S. *J. Am. Chem. Soc.* **2006**, *128*, 6034.
(8) (a) Wang, S.; Kemper, A. F.; Baldini, M.; Shapiro, M. C.; Riggs, S. C.; Zhao, Z.; Liu, Z.; Devereaux, T. P.; Geballe, T. H.; Fisher, I. R.; Mao, W. L. *Phys. Rev. B: Condens. Matter Mater. Phys.* **2014**, *89*, 245109. (b) Zhao, Z.; Zhang, H.; Yuan, H.; Wang, S.; Lin, Y.; Zeng, Q.; Xu, G.; Liu, Z.; Solanki, G. K.; Patel, K. D.; Cui, Y.; Hwang, H. Y.; Mao, W. L. *Nat. Commun.* **2015**, *6*, 7312.
(9) Goñi, A. R.; Syassen, K. In *Semiconductors and Semimetals*; Tadeusz, S., William, P., Eds.; Elsevier: Amsterdam, 1998; Vol. *54*, p 247.
(10) Jaffe, A.; Lin, Y.; Beavers, C. M.; Voss, J.; Mao, W. L.; Karunadasa, H. I. *ACS Cent. Sci.* **2016**, *2*, 201.
(11) (a) Jiang, S.; Fang, Y.; Li, R.; Xiao, H.; Crowley, J.; Wang, C.; White, T. J.; Goddard, W. A.; Wang, Z.; Baikie, T.; Fang, J. *Angew. Chem., Int. Ed.* **2016**, *55*, 6540. (b) Capitani, F.; Marini, C.; Caramazza, S.; Postorino, P.; Garbarino, G.; Hanfland, M.; Pisanu, A.; Quadrelli, P.; Malavasi, L. *J. Appl. Phys.* **2016**, *119*, 185901. (c) Szafrański, M.; Katrusiak, A. *J. Phys. Chem. Lett.* **2016**, *7*, 3458. (d) Kong, L.; Liu, G.; Gong, J.; Hu, Q.; Schaller, R. D.; Dera, P.; Zhang, D.; Liu, Z.; Yang, W.; Zhu, K.; Tang, Y.; Wang, C.; Wei, S.-H.; Xu, T.; Mao, H.-k. *Proc. Natl. Acad. Sci. U. S. A.* **2016**, *113*, 8910.
(12) Grochala, W.; Hoffmann, R.; Feng, J.; Ashcroft, N. W. *Angew. Chem., Int. Ed.* **2007**, *46*, 3620.
(13) Straus, D. B.; Hurtado Parra, S.; Iotov, N.; Gebhardt, J.; Rappe, A. M.; Subotnik, J. E.; Kikkawa, J. M.; Kagan, C. R. *J. Am. Chem. Soc.* **2016**, *138*, 13798.
(14) Zhu, X. Y.; Podzorov, V. *J. Phys. Chem. Lett.* **2015**, *6*, 4758.
(15) Jin, H.; Im, J.; Freeman, A. J. *Phys. Rev. B: Condens. Matter Mater. Phys.* **2012**, *86*, 121102.
(16) Jaffe, A.; Lin, Y.; Mao, W. L.; Karunadasa, H. I. *J. Am. Chem. Soc.* **2015**, *137*, 1673.
(17) (a) Matsuishi, K.; Suzuki, T.; Onari, S.; Gregoryanz, E.; Hemley, R. J.; Mao, H. K. *Phys. Status Solidi B* **2001**, *223*, 177. (b) Matsuishi, K.; Ishihara, T.; Onari, S.; Chang, Y. H.; Park, C. H. *Phys. Status Solidi B* **2004**, *241*, 3328.
(18) Umeyama, D.; Lin, Y.; Karunadasa, H. I. *Chem. Mater.* **2016**, *28*, 3241.
(19) Wang, L.; Wang, K.; Zou, B. *J. Phys. Chem. Lett.* **2016**, *7*, 2556.
(20) Liu, G.; Kong, L.; Gong, J.; Yang, W.; Mao, H.-k.; Hu, Q.; Liu, Z.; Schaller, R. D.; Zhang, D.; Xu, T. *Adv. Funct. Mater.* **2017**, *27*, 1604208.
(21) (a) Mitzi, D. B.; Feild, C. A.; Harrison, W. T. A.; Guloy, A. M. *Nature* **1994**, *369*, 467. (b) Mitzi, D. B.; Feild, C. A.; Schlesinger, Z.; Laibowitz, R. B. *J. Solid State Chem.* **1995**, *114*, 159. (c) Mitzi, D. B.; Wang, S.; Feild, C. A.; Chess, C. A.; Guloy, A. M. *Science* **1995**, *267*, 1473. (d) Chung, I.; Song, J.-H.; Im, J.; Androulakis, J.; Malliakas, C. D.; Li, H.; Freeman, A. J.; Kenney, J. T.; Kanatzidis, M. G. *J. Am. Chem. Soc.* **2012**, *134*, 8579.
(22) (a) Takahashi, Y.; Obara, R.; Lin, Z.-Z.; Takahashi, Y.; Naito, T.; Inabe, T.; Ishibashi, S.; Terakura, K. *Dalton Trans.* **2011**, *40*, 5563. (b) Takahashi, Y.; Hasegawa, H.; Takahashi, Y.; Inabe, T. *J. Solid State Chem.* **2013**, *205*, 39.
(23) (a) Keller, R.; Fenner, J.; Holzapfel, W. B. *Mater. Res. Bull.* **1974**, *9*, 1363. (b) Kojima, N.; Kitagawa, H.; Ban, T.; Amita, F.; Nakahara, M. *Solid State Commun.* **1990**, *73*, 743. (c) Liu, X. J.; Matsuda, K.; Moritomo, Y.; Nakamura, A.; Kojima, N. *Phys. Rev. B: Condens. Matter Mater. Phys.* **1999**, *59*, 7925.
(24) (a) Imada, M.; Fujimori, A.; Tokura, Y. *Rev. Mod. Phys.* **1998**, *70*, 1039. (b) Goodenough, J. B. *Chem. Mater.* **2014**, *26*, 820.
(25) Goodenough, J. B. *Rep. Prog. Phys.* **2004**, *67*, 1915.
(26) Ferreira, T.; Morrison, G.; Yeon, J.; zur Loye, H.-C. *Cryst. Growth Des.* **2016**, *16*, 2795.



DOI: 10.1021/jacs.7b01162
*J. Am. Chem. Soc.* XXXX, XXX, XXX−XXX